○ Discover

Research

Methane conversion to syngas by chemical looping on $La_{0.8}Sr_{0.2}Fe_xCo_{1-x}O_3$ (x = 0, 0.25, 0.50, 0.75) perovskites with CO_2 co-feeding

Gal Sror[1] · Oranit Cohen[1] · Hen Ohayon Dahan[1] · Miron V. Landau[1] · Moti Herskowitz[1]

Abstract

Partial oxidation of methane (POM) by chemical looping with CO_2 co-feeding on $La_{0.8}Sr_{0.2}FeO_3$ (LSF) perovskite catalyst yielded a highly selective operation and enabled to extend the duration of reduction cycle. In this work, the conversion of methane to syngas was studied on $La_{0.8}Sr_{0.2}Fe_{(x)}Co_{(1-x)}O_3$ (x = 0, 0.25, 0.5, 0.75) perovskites in chemical-looping mode, co-feeding CO_2 and methane. The reaction was conducted at 850 °C, 15 min reduction (10% methane in N_2, 0–3% CO_2), and 10 min oxidation (10% O_2 in N_2) cycles. The perovskites activity decreased with increasing Co content, in the absence of CO_2, due to intensified coke deposition on the catalyst. Addition of CO_2 during the reduction step (1–3%) reduced coke accumulation. A run conducted on $La_{0.8}Sr_{0.2}CoO_3$ (LSC) with continuous feeding of CO_2 and periodical (on–off) methane feeding indicated that CO_2 reacts with the accumulated coke in reverse-Boudouard reaction, increasing CO selectivity without affecting the methane conversion. XRD analysis of reduced Co-containing perovskites indicates a decreasing perovskite content. Metallic Co and La_2O_3 phases increased as the Co content in the fresh perovskite increased, increasing coke deposition. As the Co content increased, the process shifts from POM with oxygen replenishment (LSF) to cracking followed by reverse-Boudouard reaction (LSC).

1 Introduction

Natural gas, comprised primarily of methane, is used as a feedstock for syngas production [1] (a gaseous mixture of CO and H_2), to be subsequently converted to transportation fuels, chemicals, and other value-added products [2]. Partial oxidation of methane (POM) emerges as an attractive route for syngas production due to its exothermic nature [3, 4]. However, it suffers from several drawbacks [5], such as the direct interaction between gaseous oxygen and methane that creates a flammability concern, and the need for an air separation unit.

These challenges can be addressed by adopting a chemical-looping (CL) approach to the traditional POM process [6]. In CL-POM, methane reacts with lattice oxygen from a solid oxygen carrier (OC) to produce the syngas (reduction step). To close the loop, the OC is re-oxidized to its full oxygen capacity in a separate step (oxidation step). In this way, oxygen and methane contact is prevented, and the need for air separation becomes irrelevant since the oxidation can be done using air [7]. Being the exclusive oxygen source during the reduction step, the OC has a key role in CL-POM operation

---

⚡ Springer

[8]. High oxygen capacity, reactivity, and resistance to coke deposition are the key properties in the selection of OC and are essential to maximize the syngas production per cycle [9–11] For this reason, perovskite-type oxides [12] (ABO_3, A- lanthanide/alkaline earth metal, B- transition metal) are extensively employed in this operation due to their oxygen mobility, redox activity, and thermal stability. Partial or full substitution of ions in the A/B sites can improve the perovskite properties [13], promote a more selective operation, and contribute to the perovskite structure stability. Partial substitution of La^{3+} for Sr^{2+} cations in $LaFeO_3$ perovskite has been shown to improve its oxygen release performance, decreasing the lattice oxygen release energy [25, 26]. In this case, electronic imbalance in the perovskite lattice is compensated by the oxidation of a fraction of Fe^{3+} to Fe^{4+} and/or the generation of oxygen vacancies. Partial substitution of catalytically active B sites in LSF by other transition metal cations has been shown to enhance catalytic activity in syngas production due to synergistic valence changes and resultant nonstoichiometric-related microstructural defects into the lattice [27]. Major efforts are aimed at increasing the oxygen storage capacity of perovskites using various configurations to extend the effective time of syngas production at the reduction step [14–16]. Nevertheless, since the amount of oxygen available in each cycle is finite, regardless of the oxygen capacity of the OC, the CL-POM provides a discontinuous solution [17]. This intermittent operation compelled by the CL approach enables only a few minutes of methane conversion and limits the effective time of syngas production per cycle [18].

This issue has been addressed in our recent publications. Initially, a study [19] using $La_{0.8}Sr_{0.2}FeO_3$ (LSF), a perovskite with partial La substitution by Sr in the A site, revealed the beneficial effect of its combination with Fe_2O_3. Significantly improved CO selectivity was observed when the Fe_2O_3 was packed before the LSF in the catalytic reactor. This is attributed to the products of methane combustion over the Fe_2O_3 (CO_2 and steam) at 900 °C, which reach the LSF with the remaining methane. Considering this finding, which assumes the participation of these products in POM over LSF, the effect of co-feeding CO_2 with methane on the LSF performance was reported in a follow-up study [18]. It concluded that the CO_2 reacts with oxygen vacancies (O_v) in the LSF, created as the methane reacts with the lattice oxygen. This resulted in providing sufficient lattice oxygen which was restored instantly by the incoming CO_2 as demonstrated in POM with LSF [18] and with $La_{0.85}Sr_{0.15}Fe_{0.95}Al_{0.05}O_3$ perovskite [28]. Co-feeding of CO_2 yielded continuous, stable operation of PMO for 12 h [28] and 18 h [18]. Moreover, this oxygen replenishment mechanism enabled a stable operation, allowing for extended reduction times.

Substituting lattice Fe with Co in the B site of the perovskite was found to be promising for low-temp steam reforming of methane (SRM) in a study [20] that examined the combination of Co with Fe, Mn, and Ni using $LaCo_{0.6}X_{0.4}O_3$ perovskites, yielding the highest selectivity (> 90%) and H_2 purity (near 100%) at 700 °C among the tested metals. Moreover, a significant enhancement in oxygen regeneration by steam on $LaCo_{0.6}Fe_{0.4}O_3$ compared with $LaCoO_3$ was reported. Another study [7] examined the CL-SRM performance of a series of $LaFe_{(1-X)}Co_{(X)}O_3$ (X = 0.1, 0.3, 0.5, 0.7, 1.0) perovskites, concluding that a high degree of Fe substitution with Co is not beneficial for CO selectivity, but low degree improved the perovskite reactivity. Similar results were reported for low-temperature RWGS reaction with Co-substituted $LaFe_{(1-X)}Co_{(X)}O_3$ perovskite catalyst [21].

The main objective of our work was to study the effect of substituting lattice Fe with Co (in the B site of the perovskite) on the performance in CL-POM with and without CO_2 co-feeding. The effect of the Co substitution on oxygen replenishment by CO_2 was also studied.

2 Experimental

2.1 Material preparation

The perovskites were synthesized by the sol–gel method [22] LSF synthesis procedure is described in detail elsewhere [19]. The precursors of $La_{0.8}Sr_{0.2}Fe_{(X)}Co_{(1-X)}O_3$ (X = 0, 0.25, 0.5, 0.75) were dissolved in an aqueous solution at a relevant molar ratio and heated to 50 °C on a hot plate: $La(NO_3) \cdot 6H_2O$ (Sigma-Aldrich, 99.99%), $Fe(NO_3)_3 \cdot 9H_2O$ (Fluka, > 98%), $Co(NO_3)_2 \cdot 6H_2O$ (Fluka, > 98%) and ($Sr(NO_3)_2$, Fluka, > 99%) were dissolved separately in deionized water. After the precursors were fully dissolved and solutions were combined, the complexant glycine was added: 1.03 g (Sigma-Aldrich, ≥ 99%). The solution was heated to 80 °C on a hot plate until the gel formed, dried overnight at 130 °C, and calcined at 400 °C (10 °C/min) for 4 h and then at 700 °C (5 °C/min) for 2 h. XRD patterns of fresh perovskites are shown in Fig. 1.

Fig. 1 XRD patterns of fresh $(La_{0.8}Sr_{0.2})(Fe_xCo_{1-x})O_3$
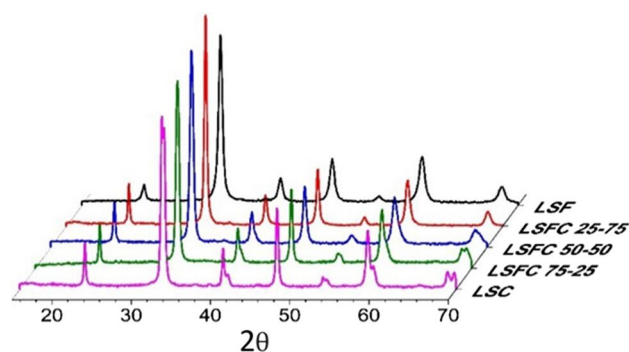
2.2 Material characterization

Fresh and spent samples were analyzed by XRD. Conventional wide-angle XRD patterns were measured with a Panalytical Empyrean Powder Diffractometer equipped with a position-sensitive X'Celerator fitted with a graphite detector monochromator (Malvern Pananalytical Ltd, Malvern, UK) at 30 mA and 40 kV. The phases were analyzed in HighScore software (Malvern Pananalytical Ltd, Malvern, UK), and the phase content was calculated using Rietveld refinement. The following entries at the database of the International Center for Diffraction Data (ICDD) were used as a reference for phase analysis: LSF (ICDD card # 35-1480), LSC (ICDD card # 82-1961), La_2O_3 (ICDD card # 5-602), metallic Co (ICDD card # 15-806), metallic Fe (ICDD card # 6-696), $SrLaFeO_4$ (ICDD card # 29-1305), $SrLaCoO_4$ (ICDD card # 83-2408), Fe_2O_3 (ICDD card # 72-469).

The surface area, pore volume, and average pore diameter of the fresh perovskites were calculated from N_2 adsorption–desorption isotherms using conventional BET (Brunauer–Emmett–Teller) and BJH (Barrett–Joyner–Halenda) methods, with NOVA 3200e Quantachrome adsorption analyzer. Before analysis, the samples were outgassed under vacuum at 250 °C for 2 h.

2.3 Experimental runs, procedures, and calculations

Chemical looping experiments were conducted in a fixed-bed described elsewhere [19]. The reactor was loaded with 1 g of perovskite particles in the size range of 180–350 μm, diluted with quartz of the same size at a 1:2 ratio. The gas composition was analyzed every 0.5 min during the run by an IR device (ABB AO2020) equipped with an infrared photometer for analysis of CO, CO_2, and methane, an oxygen analyzer (paramagnetic and thermomagnetic) for identification of O_2 and a thermal conductivity analyzer (silicon sensor and glass cell) for analysis of H_2. A typical experimental cycle is described in Table S1 and consisted of four steps: 15 min *reduction* with 10% methane (99.5%) and 0–3.0%mol CO_2 (99.5%) in N_2 (99.999%) performed at the methane weight hourly space velocity (WHSV) of 3 h^{-1} at 850–900 °C, 10 min *flushing* with N_2 (10 min), 10 min *oxidation* with 10% O_2 (99.5%) in N_2, and 10 min *purging* with N_2 (10 min). The last three steps were conducted at the same temperature as the reduction step. Experiments were also performed in a three-period configuration of reduction step with periodical methane feeding: 10% methane for 5 min, no methane for 5 min, and 10% methane for 5 min (continuous 2% CO_2).

Performance reproducibility (methane conversion, CO and H_2 selectivity) was tested at several operating conditions (LSC with 3% CO_2 at WHSV = 3 h^{-1} and 850 °C, all three LSFC perovskites with 2% CO_2 at WHSV = 3 h^{-1} and 850 °C) in 2–3 experiments, displaying ≤ 5% deviation (Figure S1 and S2 in the supplementary information). The carbon, hydrogen, and oxygen mass balances were ≥ 95%. At least 10 cycles were conducted in each experiment.

The volumetric flow rate (ml/min) of each component j was calculated from its measured gas concentration C_j:

$$v_t = \left(\frac{C_{CH_4,t} + C_{CO_2,t} + C_{H_2,t} + C_{CO,t}}{C_{CH_4,0} + C_{CO_2,0}} \right) \cdot (v_{CH_4,0} + v_{CO_2,0}) + v_{N_2,0}; v_j = C_j \cdot v_t \tag{1}$$

where, v_t is the total volumetric flow rate at the reactor outlet. $C_{CH_4,t}$, $C_{CO_2,t}$, $C_{H_2,t}$, $C_{CO,t}$ are the methane, CO_2, H_2 and CO concentration, respectively, measured by IR at the reactor outlet. $C_{CH_4,0}$ and $C_{CO_2,0}$ are the methane and CO_2 concentrations feed (10% and 1–3% mol), respectively. $v_{CH_4,0}$, $v_{CO_2,0}$ and $v_{N_2,0}$ are the volumetric flow rate of methane, CO_2 and N_2 in the feed, respectively.

The methane conversion was calculated as follows:

$$x_{CH_4,t} = \frac{F_{CH_4,0} - F_{CH_4,t}}{F_{CH_4,0}} \tag{2}$$

where $x_{CH_4,t}$ is the methane conversion at time t during the reduction cycle, $F_{CH_4,0}$ and $F_{CH_4,t}$ are the methane flowrate at the reactor inlet and at the outlet (at time t), respectively.

The CO_2 conversion was calculated as follows:

$$x_{CO_2,t} = \frac{F_{CO_2,0} - F_{CO_2,t}}{F_{CO_2,0}} \tag{3}$$

Where $x_{CO_2,t}$ is the CO_2 conversion, $F_{CO_2,0,}$ and $F_{CO_2,t}$ are the CO_2 flowrate at the reactor inlet and at its outlet at time t, respectively.

The selectivity of CO ($S_{CO,t}$) and CO_2 ($S_{CO_2,t}$) at standard CL-POM are expressed as:

$$S_{CO,t} = \frac{F_{CO,t}}{\left(F_{CH_4,0} - F_{CH_4,t}\right)} \tag{4}$$

$$S_{CO_2,t} = \frac{F_{CO_2,t}}{\left(F_{CH_4,0} - F_{CH_4,t}\right)} \tag{5}$$

where, $F_{CO,t}$ and $F_{CO_2,t}$ are the flowrates of the outlet CO and CO_2, respectively.

The selectivity of CO ($S_{CO,t}$) at CL-POM with CO_2 co-feeding is expressed as:

$$S_{CO,t} = \frac{F_{CO,t} - \left(F_{CO_2,0} - F_{CO_2,t}\right)}{\left(F_{CH_4,0} - F_{CH_4,t}\right)} \tag{6}$$

The selectivity of H_2 ($S_{H_2,t}$) and formed coke (S_{coke}) are expressed as:

$$S_{H_2,t} = \frac{F_{H_2,t}}{2(F_{CH_4,0} - F_{CH_4,t})} \tag{7}$$

$$S_{coke} = 1 - S_{CO,t} \tag{8}$$

where $F_{H_2,t}$ is the flowrate of the outlet H_2.

The amounts of CO and CO_2 produced during the reduction step were calculated as follows:

$$CO_{produced} = \int_0^t F_{CO,t} dt \tag{9}$$

$$CO_{2\,produced} = \int_0^t F_{CO_2,t} dt \tag{10}$$

The estimated amount of oxygen reacted from CO_2 was calculated as follows:

$$Reacted\,O\,from\,CO_2 = \int_0^t (F_{CO_2,0} - F_{CO_2,t}) dt \tag{11}$$

The amount of oxygen reacted during the oxidation step was calculated as follows:

$$O_{reacted} = \int_0^t 2 \cdot \left(F_{O_2,0} - F_{O_2,t}\right) dt \tag{12}$$

where $O_{reacted}$ is the amount of oxygen reacted during the oxidation step, and $F_{O_2,0}$ and $F_{O_2,t}$ are the O_2 flowrates at the reactor inlet and outlet (at time t), respectively.

The amount of oxygen that oxidized coke was calculated as follows:

$$O_{to\,coke} = \int_0^t \left(2 \cdot F_{CO_2\,oxidation,t} + F_{CO\,oxidation,t} \right) dt \qquad (13)$$

where $F_{CO_2\,oxidation,t}$ and $F_{CO\,oxidation,t}$ are the CO_2 and CO outlet flow rates during oxidation, respectively.

The estimated amount of oxygen replenished in OC from O_2 was calculated as follows:

$$Replenished\,O\,from\,O_2 = O_{reacted} - O_{to\,coke} \qquad (14)$$

The total H_2/CO ratio was calculated as follows:

$$\frac{H_2}{CO} = \frac{F_{H_2,t}}{F_{CO,t}} \qquad (15)$$

The syngas yield was calculated as follows:

$$Yield = \frac{F_{H_2,t} + F_{CO,t}}{\left(F_{CH_4,0} - F_{CH_4,t} \right)} \qquad (16)$$

3 Results and discussion

3.1 Effect of Fe substitution with Co on perovskites structure, texture, and CL-POM performance

Figure 1 shows the evolution of XRD patterns of freshly synthesized perovskites $(La_{0.8}Sr_{0.2})(Fe_xCo_{1-x})O_3$, due to changes in the structure and lattice parameters depending on the ratio of Fe/Co for each sample (Table 1).

Structure parameters listed in Table 1 indicate that the perovskites were completely crystallized at 700 °C. $(La_{0.8}Sr_{0.2})$ FeO_3 and $(La_{0.8}Sr_{0.2})(Fe_{0.75}Co_{0.25})O_3$ formed an orthorhombic perovskite phase *Pbnm* (ICDD card #35-1480) at 700 °C. $(La_{0.8}Sr_{0.2})(Fe_{0.25}Co_{0.75})O_3$ and $La_{0.8}Sr_{0.2}CoO_3$ formed the rhombohedral perovskite phase (hexagonal excise) *R-3c(h)* (ICDD card #86-1664) at 700 °C. Perovskite $(La_{0.8}Sr_{0.2})(Fe_{0.50}Co_{0.50})O_3$ represented a mixture of two structures: *Pbnm* and *R-3c(h)*. As the relative concentration of Fe ions is increased, the *V/Z* is increased (volume of perovskite lattices per part of unit cell whose atomic composition is given in Table 1 at the relevant Fe/Co composition). When the structure is rearranged from *Pbnm* to *R-3c(h)* there was an abrupt decrease in the *V/Z* value (Fig. 2).

Table 1 Structure parameters of as-prepared $La_{0.8}Sr_{0.2}Fe_{(x)}Co_{(1-x)}O_3$ (x=0, 0.25, 0.5, 0.75, 1) perovskites	Co content %	Perovskite formula	Space group	Lattice parameters			
				a	b	c	v/z
				Å	Å	Å	Å³
	0	$(La_{0.8}Sr_{0.2})FeO_3$–100% d = <20 nm>	Pbnm	5.490 (2)	5.528 (2)	7.834 (3)	59.444
	25	$(La_{0.8}Sr_{0.2})(Fe_{0.75}Co_{0.25})O_3$–100% d = <30 nm>	Pbnm	5.478 (2)	5.523 (2)	7.792 (3)	58.882
	50	$(La_{0.8}Sr_{0.2})(Fe_{0.50}Co_{0.50})O_3$–37% d = <30 nm>	Pbnm	5.461 (2)	5.523 (2)	7.792 (3)	58.132
		$(La_{0.8}Sr_{0.2})(Fe_{0.50}Co_{0.50})O_3$–63% d = <35 nm>	R-3c(h)	5.478 (2)	5.478 (2)	13.264 (3)	57.723
	75	$(La_{0.8}Sr_{0.2})(Fe_{0.25}Co_{0.75})O_3$–100% d = <35 nm>	R-3c(h)	5.460 (2)	5.460 (2)	13.232 (3)	56.937
	100	$(La_{0.8}Sr_{0.2})CoO_3$–100% d = <35 nm>	R-3c(h)	5.447 (2)	5.447 (2)	13.152 (3)	56.334

Fig. 2 Effect of Fe to Co substitution in perovskite structure on the V/Z volume of perovskite lattices per part of unit cell whose atomic composition is given in Table 1
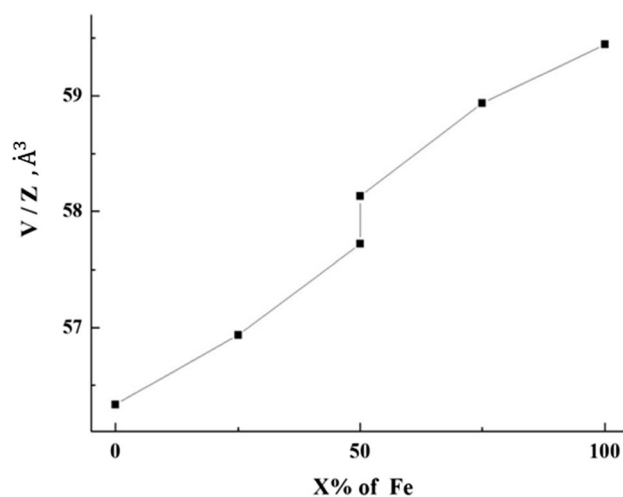
The texture characteristics of as-prepared perovskite materials are listed in Table 2. Substitution of 25% of Fe ions by Co decreased its surface area by a factor of about 4. Further gradual substitution of Fe by Co ions at the range of 25–100% did not significantly affect the surface area of the perovskite, and it remained in the range of 6–8 m^2/g. Substitution of Fe by Co ions decreased the pore volume of perovskite, increasing its average pore diameter in the whole range Co contents.

$La_{0.8}Sr_{0.2}CoO_3$ (LSC) was tested in CL-POM at 850 °C and 900 °C with 10% methane (WHSV = 3 h^{-1}). The methane conversion depicted in Fig. 3 is compared with that of LSF at 900 °C published elsewhere [19], and at 850 °C.

At the start of the cycle (0–2 min), the methane conversion obtained with LSC was higher than that measured with LSF and peaked at 65% and 42% accordingly. At > 3 min, the methane conversion on LSC dropped significantly to < 10%, in contrast to LSF. The error of the gas analyzer is ± 0.2%. At a low methane conversion (< 10%), the concentration of the other components in the outlet stream (CO_2, CO, and H_2) is very low (< 1%), making their measurement inaccurate. For this reason, performances are presented only for > 10% methane conversion. CO selectivity was significantly lower on LSC while coke selectivity was higher.

The results of XRD analysis of spent LSC after reduction step at 850 °C listed in Table 3 (complete analysis is listed in Table S2 in the supplementary information), indicate that the LSC decomposed to mainly La_2O_3 (55%), metallic Co (22.5%) and amorphous phases. The La_2O_3 phase has no active sites for POM while metallic Co enhanced methane decomposition [23] that leads to excessive coke formation and catalyst deactivation. The amorphous phase found in spent samples after experiments is represented in the XRD patterns as a wide amorphous halo centered at 2θ = 28°. The position of this halo differs from that of amorphous carbon (2θ = 26°) and corresponds to not-crystallized solid solution of metal-oxide components (La, Fe, Co), where average distance between neighbor metal ions is about 5Å.

The mixed LSFC perovskites containing both Fe and Co (25%, 50%, 75%) yielded higher methane conversion in the first 3 min, then decreasing rapidly to < 10%, as depicted in Fig. 4. As the Co content increased, CO selectivity was lower, coke selectivity was higher thus the deactivation was higher.

The change in POM activity from LSF to LSC is reflected by the gradual decrease of CO production during the reduction step (LSF—4.7 mmol/g, LSC—2.2 mmol/g). LSFC with 25% Co produced slightly more CO than the LSF (5.0 mmol/g).

Table 2 Texture characteristics of fresh perovskites

Relative Co content (%) in fresh perovskite $La_{0.8}Sr_{0.2}Fe_{(x)}Co_{(1-x)}O_3$; (1-x)	Texture characteristics (N_2-adsorption)		
	Surface area, m^2/g	Pore volume, cm^3/g	Average pore diameter, nm
0	31	0.162	20
25	8	0.044	21
50	7	0.040	23
75	6	0.041	27
100	8	0.067	34

Fig. 3 Performance of LSC and LSF at WHSV = 3 h^{-1}. **A** CH$_4$ conversion. **B** H$_2$ selectivity. **C** CO selectivity. **D** Coke selectivity
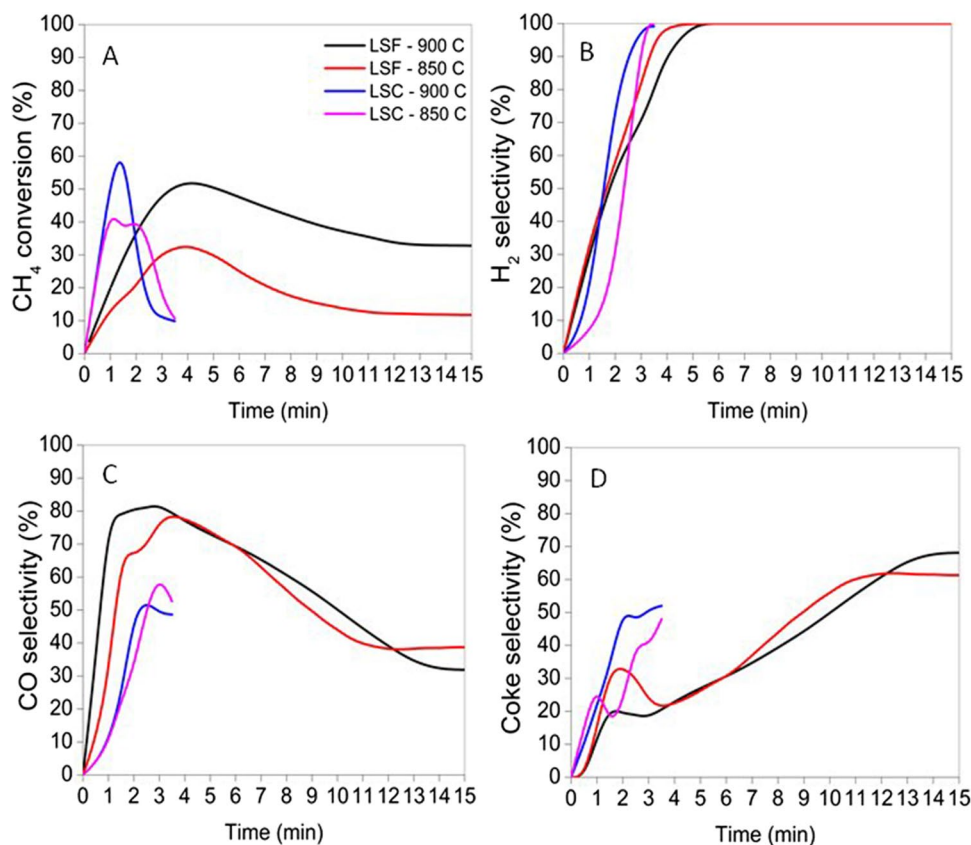

**Table 3** XRD analysis of LSC and LSFC (50–50) after 15 min reduction at 850 °C

Perovskite	Phase composition XRD (wt%/crystals size (nm))				
	Perovskite	Fe°	Co°	La$_2$O$_3$	Amorphous
LSF (900 °C, [19])	15/45	24/50	–	27/40	–
LSFC 50–50	7/20	15/35	4/35	41/40	29
LSC	2.5/30	–	22.5/40	55/40	17.5

The amounts of O reacted to CO, CO$_2$, and H$_2$O from each perovskite are listed in Table S3. The opposite trends in CO and CO$_2$ production result in a narrow range of total oxygen consumption (LSF—0.1 mmol/g, LSC—1.9 mmol/g). No major differences were observed in the amount of coke oxidized at oxidation step of the cycle (LSF—2.1 mmol/g, LSC—2.6 mmol/g). This is due to the inversed trends in methane conversion and coke selectivity as the Co content increased. Corresponding to these trends, the XRD analysis of spent 50% Co LSFC after reduction indicates that 7% of the perovskite phase remained in the structure, which is between the LSC (2.5%) and the LSF [19] (15%). In addition, 4% of metallic Co and 30% of La$_2$O$_3$ were also detected in that sample, lower than those detected in spent LSC. After oxidation step most of perovskite phase was recovered: 94% of LSF and 83% of LSC. It suggests that the increasing amount of Co in perovskite facilitates the formation of metallic cobalt phase at reaction conditions reducing the extent of POM, increasing the rate of coke formation. The formation of Fe-Co alloy was not observed in any of the spent samples.

3.2 Effect of CO$_2$ co-feeding

Co-feeding CO$_2$ with methane was reported to reduce the extent of coke deposition on LSF at 900 °C [18, 19]. Similar experiments (1–3% CO$_2$) were conducted using LSC at 850 °C and WHSV = 3 h^{-1}. The results depicted in Fig. 5 compared the LSC and LSF performance [18]. Adding CO$_2$ to the feed had a significant effect on methane conversion and selectivity.

Fig. 4 Performance of LSF, LSFC, and LSC in CL-POM at 850 °C, WHSV = 3 h^{-1}. **A** CH$_4$ conversion, **B** H$_2$ selectivity, **C** CO selectivity, **D** Coke selectivity
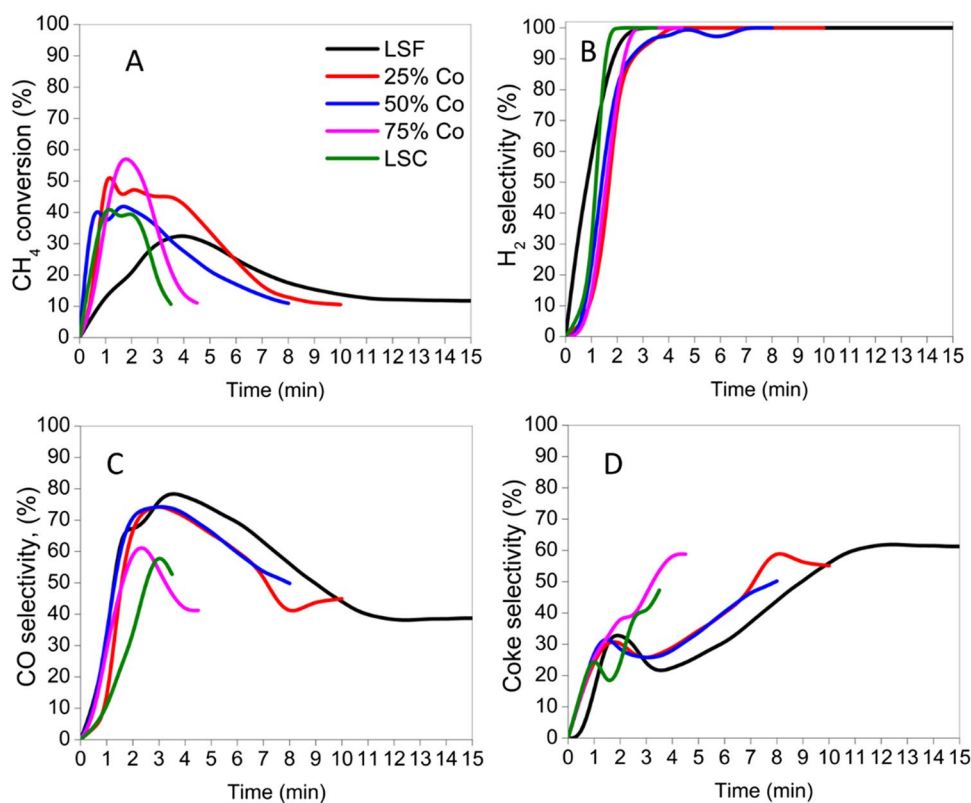
Over a transition period of 3 min, the methane and CO$_2$ conversion and the CO, H$_2$ and coke selectivity changed significantly, reaching a pseudo steady-state for the rest of the reduction stage process (3–15 min).

LSC at 850 °C displayed a remarkable increase in methane conversion (about 40%) over the tested range of CO$_2$ concentration (1–3%), higher than LSF at 900 °C with 1.6% CO$_2$. H$_2$ selectivity reached 100% and CO$_2$ conversion was complete. The CO selectivity of LSC with 1% CO$_2$ in the feed was much lower than with 3% CO$_2$ due to excessive coke formation. During the oxidation step, the amount of oxygen consumed by the LSC decreased with increasing CO$_2$ concentration (1%—5.9 mmol/g, 3%—3.1 mmol/g), as well as the amount of oxygen required to oxidize the coke accumulated during the reduction (1%—5.9 mmol/g, 3%—2.2 mmol/g). At low CO$_2$ concentration (1%), removal of coke allows more oxygen from the LSC to react, while at a higher level (3%), the coke is removed and accumulated again more rapidly (high coke turnover on the OC surface), leading to less oxygen reacted from the LSC. The same trends were observed with increasing CO$_2$ concentration using the LSF. However, with LSC the methane conversion did not change dramatically over a wide range of CO$_2$ concentrations, unlike the LSF. This indicates a different path of CO$_2$ contribution to the stable performance with LSC.

XRD analysis of spent LSC after reduction with 2% CO$_2$ (Table 4) found a negligible amount of perovskite (1.5%) in contrast with LSF (90% with 1.8% CO$_2$). The main phases in spent LSC, La$_2$O$_3$ (46%) and metallic Co (27.5%) produce coke, corresponding to the high coke selectivity during the reduction. This confirms that CO$_2$ does not replenish lattice oxygen in LSC.

The intermediate compositions perovskites were tested with 2% CO$_2$ co-feeding with 10% methane (WHSV = 3 h^{-1}) at 850 °C, 15 min reduction and 10 min oxidation time. The results are shown in Fig. 6 and compared with LSC performance under the same conditions.

The performance of 25% and 50% Co perovskites were very similar, and yielded 24% and 27% methane conversion respectively, with near 90% CO selectivity and 100% H$_2$ selectivity. A further increase in Co content in the perovskite to 75% significantly increased the methane conversion to 36% decreasing CO selectivity to 70% and increasing coke selectivity. Complete CO$_2$ conversion was achieved in all experiments. The total H$_2$/CO ratio at steady state (15 min) increased from 1.1 with 25% Co to 1.7 with LSC. This is due to the decreasing CO selectivity as the Co content increased.

These results demonstrate the gradual transition in performance of LSF to LSC at 850 °C. The CO production in the experiments described in Fig. 6 was between 17.0 to 17.7 mmol/g per cycle (Table S4), indicating a similar overall conversion of methane and CO$_2$ to CO. However, coke accumulation is intensified as Co becomes more dominant in

Fig. 5 LSC (850 °C) and LSF (900 °C) performance in CL-POM with 1–3% CO_2 co-feeding at WHSV = 3 h^{-1}. **A** CH_4 conversion, **B** H_2 selectivity, **C** H_2 selectivity, **D** Coke selectivity, **E** Syngas yield
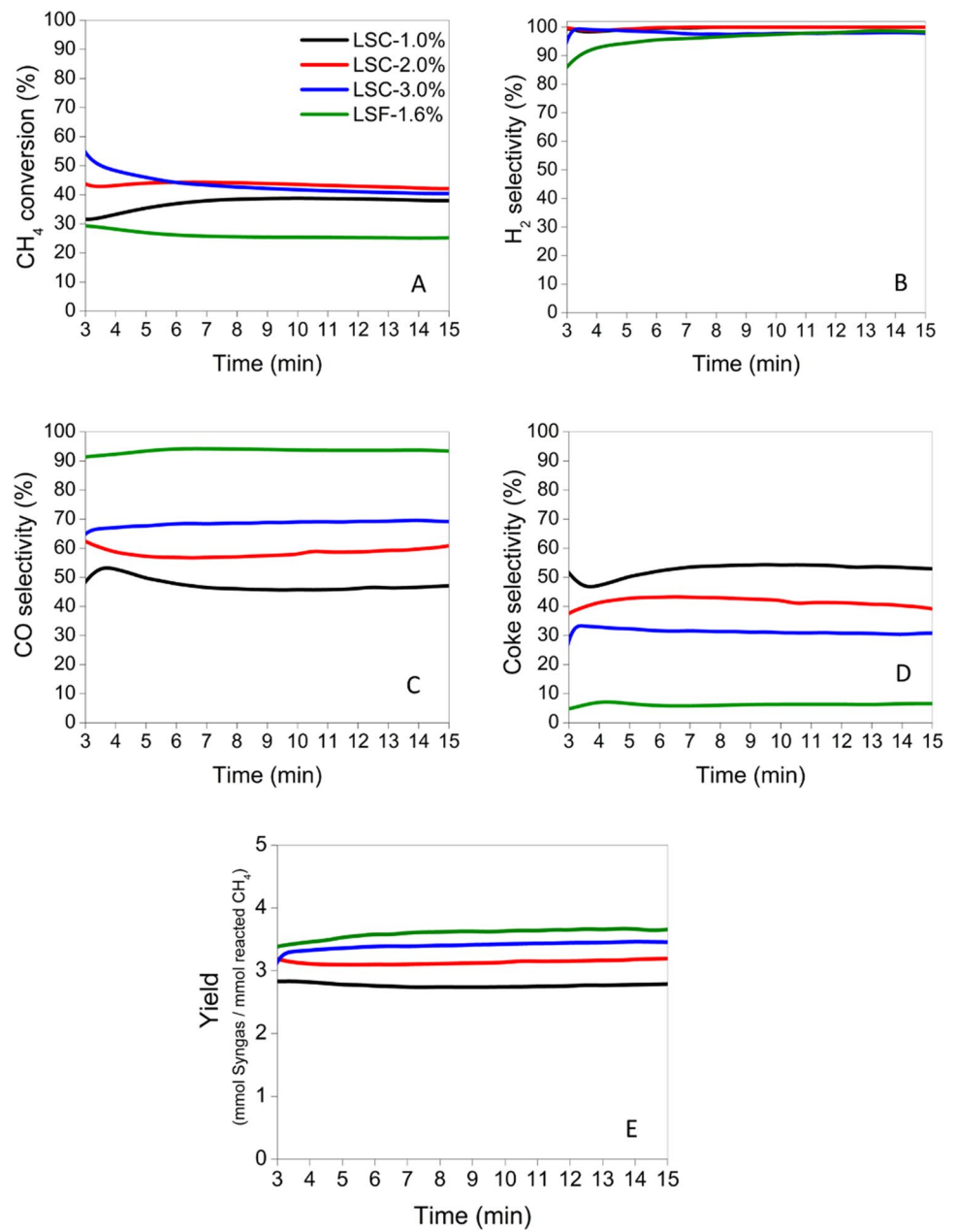

Table 4 XRD analysis of spent LSFC and LSC after reduction with 2% CO_2 co-feeding at 850 °C

Co content in fresh perovskite, %	Phase composition (XRD, wt%)/crystals size (nm)			
	Perovskite	Co°	Fe°	La_2O_3
LSF - no Co (1.8%—900 °C, [18])	90/45	–	3.5/50	–
LSFC - 25% Co	65/45	2.5/40	3/30	2.5/50
LSFC -50% Co	48/30	6/35	5/35	14/45
LSFC -75% Co	2.5/45	19/35	7/40	36.5/45
LSC - 100% Co	1.5/30	27.5/45	–	46/45

Fig. 6 LSFC performance in CL-POM with 2% CO_2 co-feeding at 850 °C and WHSV = 3 h^{-1}. **A** CH_4 conversion, **B** H_2 selectivity, **C** CO selectivity, **D** Coke selectivity, **E** Syngas yield
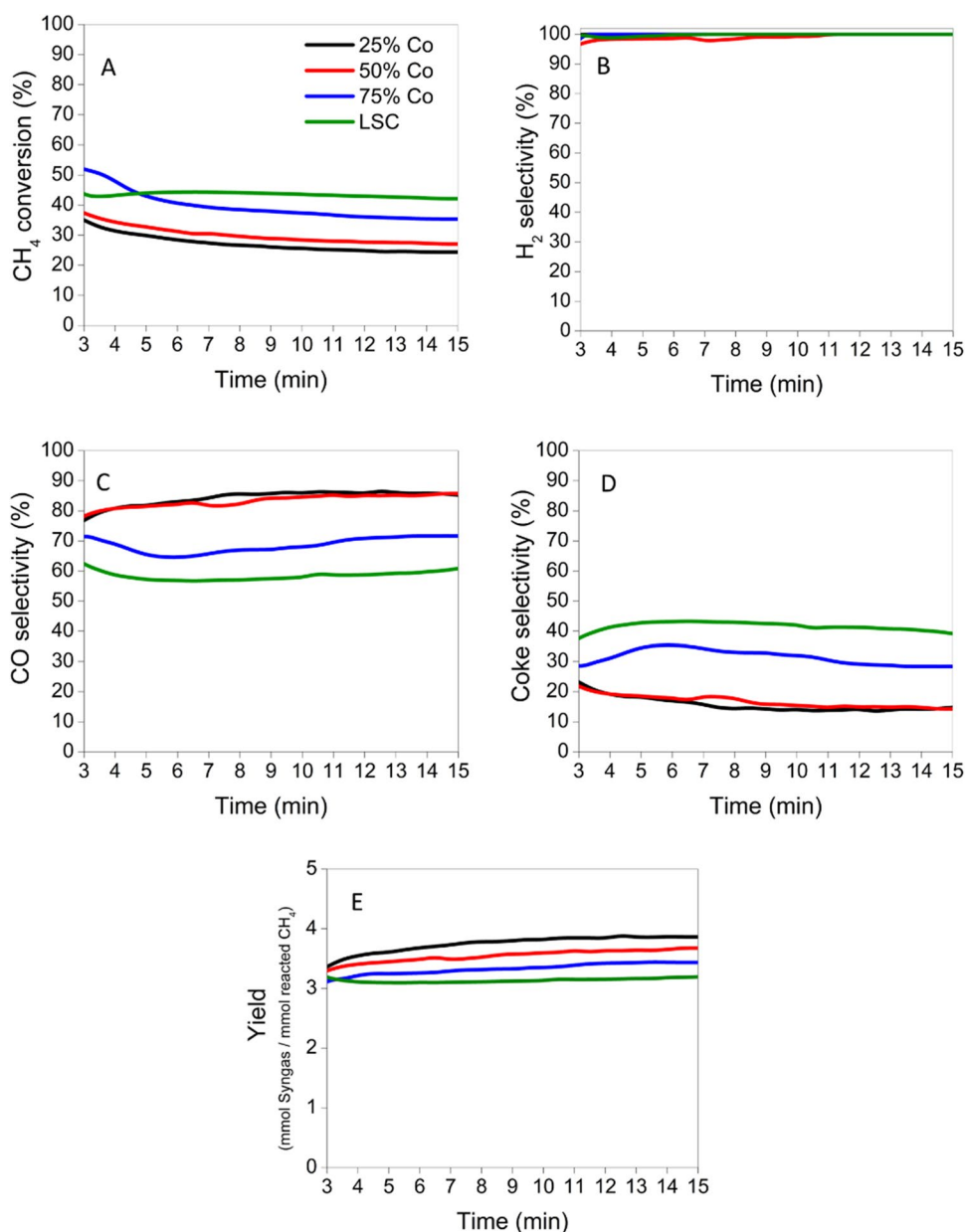
the perovskite, leading to higher methane conversions and a lower CO selectivity as Co content in the perovskite increases. Correspondingly, the amount of oxygen required to combust the coke during the oxidation step increased with increasing Co content (25% Co—0.2 mmol/g, LSC—4.6 mmol/g).

XRD analysis of the intermediate compositions indicates a decrease in the amount of perovskite phase with increasing Co content after reduction with 2% CO_2 (Table 4). This confirms the decreasing extent of oxygen replenishment. However, the amount of metallic Co and La_2O_3 increased, corresponding to the increase in coke selectivity. Since not all Fe and Co in LSFC perovskites were reduced to metallic state (some remained in non-reduced perovskite phase) the amounts of metallic Fe and Co in the spent samples do not correspond to the ratio of Fe and Co in the fresh perovskite. Rietveld refinement example is shown in Figure S3, complete XRD analysis is listed in Table S5.

There are two feasible routes for the CO_2 reaction, yielding two CO and two H_2 molecules. The first is a direct reaction between methane and CO_2 (dry reforming). The second is a series of consecutive reactions involving coke deposition according to methane cracking followed by a reverse-Boudouard reaction, in which the coke is converted to CO by reacting with CO_2 [24].

The reversibility effect of CO_2 on the LSC performance and its reaction with coke was examined in a three-period run during the reduction cycle: 10 mol% methane and 2 mol% CO_2 for 5 min, no methane for 5 min, and 10 mol% methane and 2 mol% CO_2 for 5 min. The results are shown in Fig. 7.

As expected, none of the methane reactions occurred during period 2. 1.6 mmol CO_2 reacted with an equivalent amount of coke to produce 3.2 mmol CO in this period (subplot 7B, period 2). This confirms unequivocally that reverse-Boudouard reaction occurs ($C + CO_2 \rightarrow 2CO$). At the beginning of period 3, 0.6 mmol of CO_2 were detected between 10–11 min (subplot 7B, period 3), followed by the production of 5.5 mmol CO (subplot 7C, period 3). This is due to the coke removal in period 2, exposing more oxygen to react with the methane. Furthermore, the oxygen consumption by the OC during the oxidation step in the three-period reduction was higher (7.2 mmol) compared with the constant feed (4.4 mmol), although less methane was introduced to the system. This is because more oxygen from the OC was exposed to react with methane in period 3, leading to more oxygen required to achieve full replenishment during the oxidation step.

Fig. 7 LSC performance in three-periods experiment at 850 °C and WHSV = 3 h^{-1}. A CH_4 conversion, B CO_2 conversion, C CO selectivity, D H_2 selectivity, E Coke selectivity
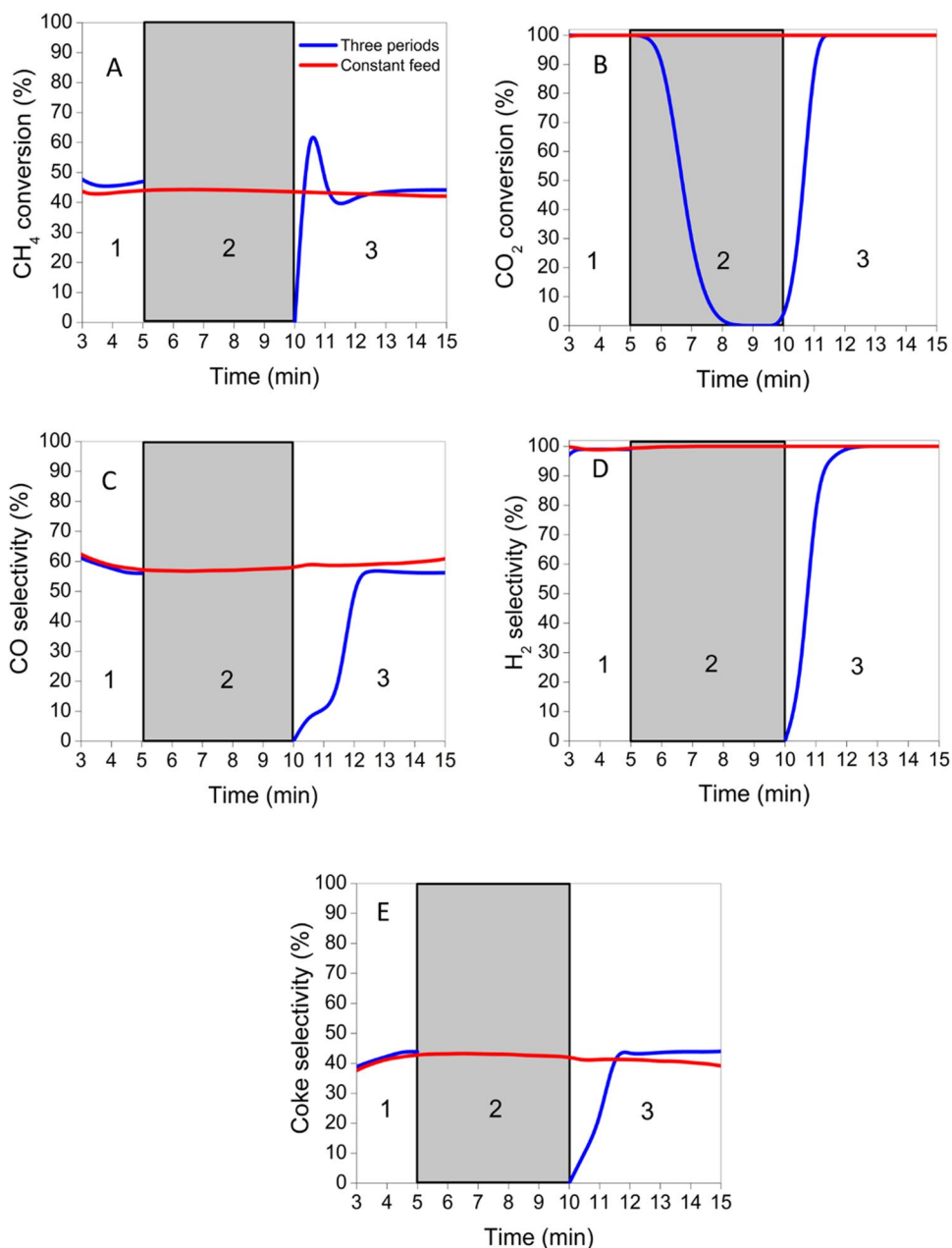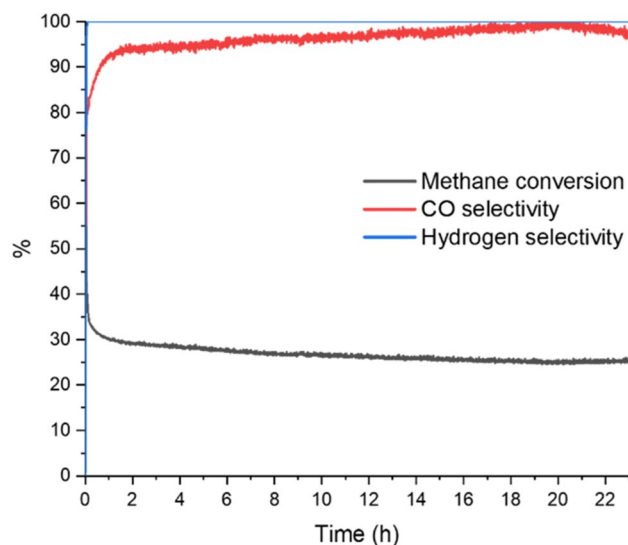
Fig. 8 LSFC performance in a continuous run at 850 °C and WHSV = 3 h^{-1} with 2% CO_2

Finally, a continuous run (23 h) was conducted with LSFC 50–50, to prove the removal of coke that leads to stable performance. The run was conducted at 850 °C and WHSV = 3 h^{-1} with 2% CO_2. The run started after the LSFC was fully oxidized, without oxidative regeneration throughout the experiment. The result is depicted in Fig. 8.

The CO_2 conversion was complete starting at 3 min in the run. Stable performance was measured within the first hour, with methane conversion of 30% and CO selectivity of 93%. The H_2 selectivity reached 100% within 5 min. As the run progressed, an increase in the CO selectivity was observed, reaching near 100% towards the end of the run. This result confirms the continuous removal of coke from the OC surface by the CO_2 via the reverse-Boudouard reaction, leading to a stable, highly selective syngas production.

4 Conclusions

The conversion of methane to syngas was conducted over $La_{0.8}Sr_{0.2}Fe_{(x)}Co_{(1-x)}O_3$ (x = 0, 0.25, 0.5, 0.75) perovskites in chemical-looping with and without CO_2 co-feeding during the reduction step. As the Co content in the perovskite increased, POM activity was inhibited by intensified coke deposition. This is attributed to the transformation of the perovskite structure to metallic Co and La_2O_3, as revealed by XRD analysis. With CO_2 co-feeding, coke selectivity decreased with increasing CO_2 concentration (1–3%) on $La_{0.8}Sr_{0.2}CoO_3$ (LSC), but the methane conversion was not affected, unlike the behavior observed with $La_{0.8}Sr_{0.2}FeO_3$ (LSF), as observed in our previous study [18]. This different performance is related to the reverse-Boudouard reaction, reducing coke selectivity and increasing CO selectivity without a significant change in the methane conversion. This resulted in stable performance over 15 min reduction due to the continuous conversion of methane to coke followed by the conversion of the coke to CO by CO_2. The intermediate composition perovskites (x = 0.25, 0.5, 0.75) display a combination of the oxygen replenishment mechanism and the reverse-Boudouard, performing in the range between LSF and LSC. Ultimately, a continuous run (23 h) conducted with LSFC 50–50 yielded stable performance at 850 °C. Despite the different mechanisms of LSF and LSC, the outcome is a highly selective operation (> 95% CO selectivity) at a lower operating temperature compared with the LSF (900 °C).

Data availability The datasets generated during and/or analyzed during the current study are available from the corresponding author on reasonable request.

Declarations

Competing interests The authors declare no competing interests.

Open Access This article is licensed under a Creative Commons Attribution 4.0 International License, which permits use, sharing, adaptation, distribution and reproduction in any medium or format, as long as you give appropriate credit to the original author(s) and the source, provide a link to the Creative Commons licence, and indicate if changes were made. The images or other third party material in this article are included in the article's Creative Commons licence, unless indicated otherwise in a credit line to the material. If material is not included in the article's Creative Commons licence and your intended use is not permitted by statutory regulation or exceeds the permitted use, you will need to obtain permission directly from the copyright holder. To view a copy of this licence, visit http://creativecommons.org/licenses/by/4.0/.

References

1. Schwach P, Pan X, Bao X. Direct conversion of methane to value-added chemicals over heterogeneous catalysts: challenges and prospects. Chem Rev. 2017;117(13):8497–520. https://doi.org/10.1021/acs.chemrev.6b00715.
2. Kee RJ, Karakaya C, Zhu H. Process intensification in the catalytic conversion of natural gas to fuels and chemicals. Proc Combust Inst. 2017;36(1):51–76. https://doi.org/10.1016/j.proci.2016.06.014.
3. Elbadawi AH, Ge L, Li Z, Liu S, Wang S, Zhu Z. Catalytic partial oxidation of methane to syngas: review of perovskite catalysts and membrane reactors. Catal Rev Sci Eng. 2021;63(1):1–67. https://doi.org/10.1080/01614940.2020.1743420.
4. Christian Enger B, Lødeng R, Holmen A. A review of catalytic partial oxidation of methane to synthesis gas with emphasis on reaction mechanisms over transition metal catalysts. Appl Catal A. 2008;346(1):1–27. https://doi.org/10.1016/j.apcata.2008.05.018.
5. Li K, Wang H, Wei Y, Yan D. Syngas production from methane and air via a redox process using Ce–Fe mixed oxides as oxygen carriers. Appl Catal B. 2010;97(3):361–72. https://doi.org/10.1016/j.apcatb.2010.04.018.
6. Bhavsar S, Veser G. Chemical looping beyond combustion: production of synthesis gas via chemical looping partial oxidation of methane. RSC Adv. 2014;4(88):47254–67. https://doi.org/10.1039/C4RA06437B.
7. Zhao K, He F, Huang Z, et al. Perovskite-type oxides LaFe$_{1-x}$Co$_x$O3 for chemical looping steam methane reforming to syngas and hydrogen co-production. Appl Energy. 2016;168:193. https://doi.org/10.1016/j.apenergy.2016.01.052.
8. Zhu X, Imtiaz Q, Donat F, Müller CR, Li F. Chemical looping beyond combustion: a perspective. Energy Environ Sci. 2020;13(3):772–804. https://doi.org/10.1039/C9EE03793D.
9. Kang Y, Han Y, Tian M, et al. Promoted methane conversion to syngas over Fe-based garnets via chemical looping. Appl Catal B. 2020;278:119305. https://doi.org/10.1016/j.apcatb.2020.119305.
10. Zagaynov IV. Active components of catalysts of methane conversion to synthesis gas: brief perspectives. Energy Fuels. 2021;35(11):9124–36. https://doi.org/10.1021/acs.energyfuels.1c00219.
11. Yan Y, Xu L, Wang L, et al. Syngas production from chemical-looping reforming of methane using iron-doped cerium oxides. Energy Technol. 2018;6(9):1610–7. https://doi.org/10.1002/ente.201700884.
12. Zeng L, Cheng Z, Fan JA, Fan L, Gong J. Metal oxide redox chemistry for chemical looping processes. Nat Rev Chem. 2018;2(11):349–64. https://doi.org/10.1038/s41570-018-0046-2.
13. Li D, Xu R, Gu Z, Zhu X, Qing S, Li K. Chemical-Looping conversion of methane: a review. Energy Technol. 2019. https://doi.org/10.1002/ente.201900925.
14. Ohayon Dahan H, Landau MV, Vidruk Nehemya R, et al. Core-shell Fe$_2$O$_3$@La$_{1-x}$Sr$_x$FeO$_{3-\delta}$ material for catalytic oxidations: coverage of iron oxide core, oxygen storage capacity and reactivity of surface oxygens. Materials. 2021;14(23):7355. https://doi.org/10.3390/ma14237355.
15. Neal LM, Shafiefarhood A, Li F. Dynamic methane partial oxidation using a Fe$_2$O$_3$@La$_{1-x}$Sr$_x$FeO$_{3-\delta}$ Core-Shell redox catalyst in the absence of gaseous oxygen. Acs Catal. 2014;4(10):3560–9. https://doi.org/10.1021/cs5008415.
16. Shafiefarhood A, Galinsky N, Huang Y, Chen Y, Li F. Fe$_2$O$_3$@La$_{1-x}$Sr$_x$FeO$_{3-\delta}$ core-shell redox catalyst for methane partial oxidation. ChemCatChem. 2014;6(3):790–9. https://doi.org/10.1002/cctc.201301104.
17. Sun Y, Li C, Djerdj I, et al. Oxygen storage capacity versus catalytic activity of ceria–zirconia solid solutions in CO and HCl oxidation. Catal Sci Technol. 2019;9(9):2163–72. https://doi.org/10.1039/C9CY00222G.
18. Ohayon Dahan H, Sror G, Landau MV, Edri E, Herskowitz M. Selective partial oxidation of methane with CO$_2$ using mobile lattice oxygens of LSF. ACS Eng. 2023. https://doi.org/10.1021/acsengineeringau.3c00008.
19. Ohayon Dahan H, Sror G, Landau MV, Herskowitz M. Chemical looping reaction of methane with oxygen from La$_{1-x}$Sr$_x$FeO$_{3-\delta}$ and La$_{1-x}$Sr$_x$FeO$_{3-\delta}$-Fe$_2$O$_3$ systems to syngas. Discov Chem Eng. 2022. https://doi.org/10.1007/s43938-022-00010-5.
20. Lee M, Lim HS, Kim Y, Lee JW. Enhancement of highly-concentrated hydrogen productivity in chemical looping steam methane reforming using Fe-substituted LaCoO$_3$. Energy Convers Manage. 2020;207:112507. https://doi.org/10.1016/j.enconman.2020.112507.
21. Pomiro FJ, Fouga GG, Bohé AE, De Micco G. CO$_2$ conversion to CO by LaCo$_{1-x}$Fe$_x$O$_3$ perovskite phases at low temperature. J Alloys Compd. 2023. https://doi.org/10.1016/j.jallcom.2022.168671.
22. Zhong Z, Chen K, Ji Y, Yan Q. Methane combustion over B-site partially substituted perovskite-type LaFeO$_3$ prepared by sol-gel method. Appl Catal A. 1997;156(1):29. https://doi.org/10.1016/s0926-860x(97)00003-3.
23. Cunha AF, Mahata N, Órfão JJM, Figueiredo JL. Methane decomposition on La$_2$O$_3$-promoted Raney-type Fe catalysts. Energy Fuels. 2009;23(8):4047–50. https://doi.org/10.1021/ef900385e.
24. Tsipouriari VA, Verykios XE. Carbon and oxygen reaction pathways of CO$_2$ reforming of methane over Ni/La$_2$O$_3$ and Ni/Al$_2$O$_3$ catalysts studied by isotopic tracing techniques. J Catal. 1999;187(1):85–94. https://doi.org/10.1006/jcat.1999.2565.

25. Wang X, Krzystowczyk E, Dou J, Li F. Net electronic charge as an effective electronic descriptor for oxygen release and transport properties of $SrFeO_3$-Based oxygen sorbents. Chem Mat. 2021;33(7):2446–56. https://doi.org/10.1021/acs.chemmater.0c04658.

26. Mishra A, Li T, Li F, Santiso EE. Oxygen vacancy creation energy in Mn-containing perovskites: an effective indicator for chemical looping with oxygen uncoupling. Chem Mat. 2019;31(3):689–98. https://doi.org/10.1021/acs.chemmater.8b03187.

27. Nalbandian L, Evdou A, Zaspalis V. $La_{1-x}Sr_xM_yFe_{1-y}O_{3-\delta}$ perovskites as oxygen-carrier materials for chemical-looping reforming. Int J Hydrog Energy. 2011;36(11):6657–70. https://doi.org/10.1016/j.ijhydene.2011.02.146.

28. Ugwu A, Zaabout A, Donat F, et al. Combined syngas and hydrogen production using gas switching technology. Ind Eng Chem Res. 2021;60(9):3516–31. https://doi.org/10.1021/acs.iecr.0c04335.